Theory of the liquid film motor

M. S. Feiz,[1] R. M. Namin,[2,*] and A. Amjadi[1]
[1]*Physics Department, Sharif University of Technology, Tehran, Iran*
[2]*Department of Mechanical Engineering, Sharif University of Technology, Tehran, Iran*
(Received 11 February 2015; published 2 September 2015)

The liquid film motor is a freely suspended liquid film placed between two capacitively coupled plates that rotates when an electric current is passed through it. Here we propose a theory for its rotation mechanism based on thin film electroconvection. The capacitively coupled plates induce free charges on the surfaces of the film, and the electric field on the film exerts a force that induces rotation. Results of the proposed theory and simulation are in good agreement with the experiments in different properties of the liquid film motor.

DOI: 10.1103/PhysRevE.92.033002 PACS number(s): 47.65.−d, 47.15.gm, 68.15.+e

I. INTRODUCTION

Properties of freely suspended liquid films have been of interest in the past century in studies regarding soap films and soap bubbles [1–7]. Their two-dimensional (2D) dynamical behavior offers an experimental medium for the investigation of physics of two-dimensional systems [8–11], which becomes especially interesting in the case of films of liquid crystals, where the film thickness is quantized to one or more molecular layers. [12–14].

A remarkable phenomenon in this context is the electroconvection in suspended liquid films, which has been extensively studied in the past decades [15–27]. It is an instability caused in the freely suspended liquid film when an electric current passes through it. Many experiments and theoretical studies have been performed regarding the electroconvection phenomenon, and as a result the governing equations regarding the dynamics of thin films in the presence of electric fields are well known. The electrical instability in a thin film creates a motion similar to thermal convection if the field is strong enough, forming cells of counter rotating flows (similar to Benard cells). The convection is encountered because of the force exerted to free charges accumulated on the surface of the film.

Amjadi *et al.* [28] reported a novel phenomenon: They conducted an electric current through a horizontal freely suspended liquid film, and placed it between two large vertical plates, connected to a high-voltage power supply. As a result, a rotation was observed with a well-defined predictable direction. This was named the liquid film motor. Later other experiments were also carried out in similar arrangements, with many different liquids and also liquid crystals to find out more about its dynamical mechanism [29,30]. Recently, it was found that this motor can act reversely to form an electric generator, and the effect was named the liquid film electric generator [31]. Similar effects are explained in old papers of Electrohydrodynamics. For example, the review paper by Melcher and Taylor [32] describes well the effect of interfacial shear stresses. The effects discussed therein are closely related to the dynamics of the liquid film motor, where similarly external electrodes induce surface charges on the interface, and the electric field creates a shear force, inducing fluid motion.

After reporting the liquid film motor, two hypothesis were given to explain its rotation mechanism. Shiryaeva *et al.* [33] assumed that free charges are accumulated at the edges of the film, and the internal electric field exerts a force that leads to a slip velocity at the sides. The slip velocity in this model was similar to the electro-osmotic slip caused by charges within the Debye length near the edges [34,35]. This explanation was not in agreement with the experiments since experimental results showed a no-slip boundary at the edges and that the maximum velocity of motion occurred somewhere between the center and sides of the film [29]. The main problem with this theory [33] was the assumption that free charges are induced near the edges only, and the free surfaces of the film are charge-free. This assumption comes from a two-dimensional picture, while recalling from the literature on thin film electroconvection, it is quite clear that a three-dimensional (3D) equation must be solved to understand the electrostatics of such systems. Free charges are induced all over the free surfaces of the film and not at the edges only. Liu *et al.* [36,37] suggested another explanation, which was based on the continuous competition between the destruction and the reestablishment of the polarization equilibrium. This hypothesis is inconsistent with the previous literature on electroconvection (e.g., Refs. [15,17,19–27,38]). Also, many experimental results, such as the effect of conductivity on the motion and the form of motion in weakly conducting liquids [29] cannot be explained with this theory.

In this paper we present a theory on the liquid film motor based on the governing equations derived for thin film electroconvection. The phenomenon and the rotation mechanism is qualitatively explained in Sec. II and the governing equations are derived in Sec. III. A numerical solution on motion equations using a finite difference method is performed, as explained in Sec. IV. In Sec. V, numerical results are presented, discussed, and compared with experimental results, showing that they are in good agreement. Finally conclusions are presented in Sec. VI.

II. PHENOMENON EXPLANATION

The experiment setup consists of a two-dimensional horizontal frame lying in the x-y plane on which the suspended film is formed (Fig. 1). Two sides of the frame are conductive and act as a conducting electrode, which when a voltage of V_{in} is applied to it, creates an average electric field of $\boldsymbol{E}_{\text{in}}$ inside

*namin@mech.sharif.edu

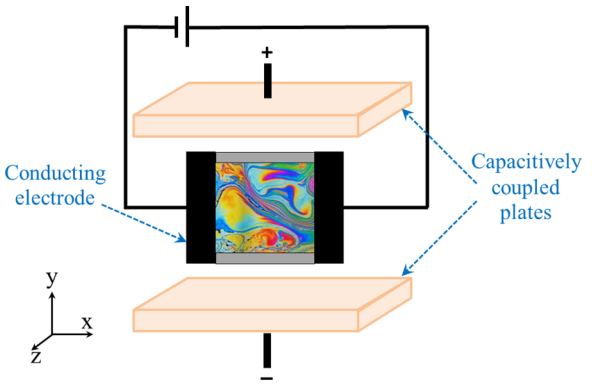

FIG. 1. (Color online) Schematic of the experiment setup.

the film and conducts an electrical current through the film in the negative x direction. The system is placed between two capacitively coupled plates connected to a high-voltage power supply. If the film was not present, these plates would produce a uniform electric field E_{ex} in the negative y direction. When the film is present, it changes the field in its immediate vicinity and a uniform external field will only be found far from the film.

When both voltages are applied, the film starts to rotate steadily in its plane, if the electric fields are of sufficient magnitude. The direction of rotational velocity is in the direction of $\boldsymbol{E}_{\text{ex}} \times \boldsymbol{E}_{\text{in}}$. This fact about the direction was observed to be consistent for all of the rotating liquids and has never been violated in experiments. For details about the experiments see Refs. [28] and [29].

The device has been tested for several liquids, showing that the liquids that are conductive and have polar molecules are able to rotate. It was reported that the conductivity itself does not necessarily change the rotational behavior. For example, for water-soap films, adding salt (e.g., NaCl) did not change the rotational characteristics while the conductivity was greatly altered. This fact has been interpreted before [28,29] to conclude that explanations that are based on conduction and the surface charge mechanisms cannot be true. However, we explain here that this observation does not lead to the rejection of such explanations.

It was shown [39] that in experiments with a bulk of liquid, the rotation is initiated at the free surface, which shows that the phenomenon is surface dominated. A bulky liquid has a much weaker rotation than a thin film because of this effect.

Our explanation relies on the surface charges induced by the conducting electrodes and the capacitively coupled plates. It is essential to understand that when the film is subjected to each of the voltages, charges are accumulated all over the free surfaces (liquid-air interfaces) and not on the edges only. With the conducting electrodes, positive charges are accumulated near the positive electrode and vice versa. With the capacitively coupled plates it is the inverse; as negative charges are induced near the positive plates and vice versa. The liquid is an ohmic conductor, thus the electric field inside it is proportional to the conductive current density. The local electric field $\boldsymbol{E}$ exerts a surface force $\boldsymbol{F}$ to the liquid with a surface charge density of q: $\boldsymbol{F} = q\boldsymbol{E}$. This force is the main driving force of the rotation of the film motor. According to this explanation, the main role of the capacitively coupled plates is to induce charge density gradient along the y direction, and the internal voltage creates a current in the film in the negative x direction. This configuration leads to an asymmetric force and is responsible for the rotation in the liquid film motor. The resulted direction of rotation here is just the same as in the experimental observations.

Based on this explanation the effect of conductivity (σ) can be understood. There are two mechanisms for charge transport; Conductive current $\boldsymbol{j}_{\text{con}} = \sigma \boldsymbol{E}$ and advection $\boldsymbol{j}_{\text{adv}} = q\boldsymbol{u}$, where $\boldsymbol{u}$ is the fluid velocity. Assuming that fluid velocity is zero in the film, in the presence of the electric voltages, there is a stable charge distribution for the film, which we call the base charge state $q_0(x,y)$. The conductivity value has no effect on this base charge state, but the time it takes from the moment the fields are applied until the formation of the base state is a function of conductivity (electrical relaxation time τ_E). In the general case when the film is in motion, the distribution of charges is affected by the advection term. The variation in the charge distribution by this effect is in direct relation to the velocity magnitudes and inversely proportional to the conductivity. Thus if the conductivity is high enough, the state of charges and potentials will be similar to the base state. However, if conductivity is low, the charge distribution will be affected by the motion. This argument is why increasing water's conductivity did not change the rotation behavior in experiments, since according to our explanation in the coming sections, water would have a high conductivity and the charge distribution would not be affected by motion. This idea is made more clear later in the theory where a dimensionless ratio, the Prandtl-like number, will be introduced, which makes this argument more precise.

III. GOVERNING EQUATIONS

The film is confined to a square frame of side dimensions of a. The thickness of the film h is several orders of magnitude smaller than a (h is less than 1 μm in the experiments while a is several millimeters or centimeters), therefore the dynamics can be modeled two-dimensionally. The dynamics is essentially surface dominated and the ratio of bulk to surface forces on the film is $O(h/a) \approx 10^{-5}$ [26]. The origin of the Cartesian coordinate system is assumed to be at the center of the film, so the film is located in $-a/2 < y < a/2$, $-a/2 < x < a/2$ and $z = 0$. There are two conducting electrodes connected to the film. One occupies the region $x > a/2$, $-a/2 < y < a/2$ and the other occupies the region $x < a/2$, $-a/2 < y < a/2$. The capacitively coupled plates are two large parallel vertical plates separated in the y direction, each having a distance of $D/2$ from the center of the film ($D \gg a$). The plates have a voltage of $\pm V_{\text{ex}}/2$. The magnitude of the external electric field as defined before would be $E_{\text{ex}} = V_{\text{ex}}/D$. The fluid has a two-dimensional mass density of ρ, viscosity of μ, and conductivity of σ, each being related to their 3D counterparts by a factor of thickness h.

Recalling from the literature on electroconvection [38], the governing equations addressing electrohydrodynamics in suspended thin liquid films are as follows. In this context, magnetic forces and dielectric effects are negligible:

$$\nabla \cdot \boldsymbol{u} = 0 \tag{1}$$

$$\rho\left(\frac{\partial \boldsymbol{u}}{\partial t}+(\boldsymbol{u}\cdot\boldsymbol{\nabla})\boldsymbol{u}\right)=-\boldsymbol{\nabla}P+\mu\nabla^2\boldsymbol{u}+q\boldsymbol{E}, \tag{2}$$

$$\frac{\partial q}{\partial t}=-\boldsymbol{\nabla}\cdot(\sigma\boldsymbol{E}+q\boldsymbol{u}), \tag{3}$$

$$q=-2\epsilon_0\partial_z\psi_3|_{z=0^+}, \tag{4}$$

$$\nabla_3^2\psi_3=\nabla_2^2\psi_3+\frac{\partial^2\psi_3}{\partial z^2}=0, \tag{5}$$

$$\psi_2=\psi_3(z=0). \tag{6}$$

The first two equations are the continuity and momentum of Navier-Stokes equations, in which $\boldsymbol{u}$ is the fluid velocity, P is pressure, q is surface charge density, and $\boldsymbol{E}$ is the electric field in the fluid, which is related to the potential on the film by $\boldsymbol{E}=-\boldsymbol{\nabla}_2\psi_2$. In the second equation, the electric charge multiplied by the electric field is a driving force and therefore is a source of momentum. The third equation is the conservation of charge, which is transferred by an ohmic conduction term $\sigma\boldsymbol{E}$ and an advection term $q\boldsymbol{u}$. ϵ_0 is the vacuum permittivity. The subscripts denote two- and three-dimensional potentials and gradients. The 2D charge density q obeys Eq. (4), a Maxwell equation that describes the nonlocal relationship between the charge density and the potential on the film ψ_2. The factor of 2 in Eq. (4) corresponds to two (upper and lower) free surfaces of the film. The 3D potential outside the film ψ_3 obeys a Laplace Eq. (5), since there are no free charges outside the film. Equation (6) expresses the fact that the electric potential is continuous everywhere, so the 2D potential on the film ψ_2 is equal to the 3D potential ψ_3 in the representative point. Thus, Eq. (4) acts as a boundary condition for Eq. (5), therefore having the charge distribution on the film, these equations could result in finding the potentials on the film and in the 3D space above.

The fluid velocity is subject to a no-slip boundary condition at the edges of the film. Although this assumption is argued in the theory of Shiryavea *et al.* [33] for the liquid film motor, the no-slip behavior is directly observable in the experiments. The potential ψ_2 is $-V_{\text{in}}/2$ on one electrode and $V_{\text{in}}/2$ on the other electrode.

To simplify the fluid dynamics, we employed the stream-function-vorticity formulation for the primitive variables in the simulation. The stream function ϕ and vorticity ω are defined in 2D as [22]

$$\boldsymbol{u}=\boldsymbol{\nabla}\phi\times z,\quad \boldsymbol{\nabla}\times\boldsymbol{u}=\omega z. \tag{7}$$

With the stream-function-vorticity formulation, the pressure will be eliminated from the calculations and the unknown velocity vector field in Eqs. (1) and (2) will be replaced by the two simpler scalar fields, ω and ϕ.

To derive dimensionless equations, we rescaled lengths with the film dimensions a, time with the viscose relaxation time $\tau_v=\rho a^2/\mu$, electric potential with the mean voltage $V_m=\sqrt{V_{\text{in}}E_{\text{ex}}a}$, and charge density with $\varepsilon_0 V_m/a$. We obtain the following dimensionless governing equations:

$$\nabla^2\phi=-\omega, \tag{8}$$

$$\frac{\partial\omega}{\partial t}+(\boldsymbol{u}\cdot\boldsymbol{\nabla})\omega=\nabla^2\omega+\mathcal{F}\boldsymbol{\nabla}\times(q\boldsymbol{E}), \tag{9}$$

$$\frac{\partial q}{\partial t}+(\boldsymbol{u}\cdot\boldsymbol{\nabla})q=\frac{1}{\mathcal{P}}\nabla^2\psi_2, \tag{10}$$

$$\nabla_3^2\psi_3=0,\quad q=-2\partial_z\psi_3|_{z=0^+} \tag{11}$$

$$\psi_2=\psi_3(z=0). \tag{12}$$

The important dimensionless parameters in this phenomenon are

$$\mathcal{F}\equiv\frac{\rho a\varepsilon_0 V_m^2}{\mu^2},\quad \mathcal{P}\equiv\frac{\varepsilon_0\mu}{\rho a\sigma},\quad \text{and}\quad \mathcal{C}\equiv\frac{aE_{\text{ex}}}{V_{\text{in}}}. \tag{13}$$

The main control parameter, $\mathcal{F}$, is a measure of the relative strength of applied electric forcing to viscose dissipation. $\mathcal{P}$ is a fluid parameter that characterizes the ratio of electric relaxation time ($\tau_E=\varepsilon_0 a/\sigma$) to viscose relaxation time and in the case of electroconvection, it is named the Prandtl-like number because of the analogy to Rayleigh-Benard convection. The other control parameter is $\mathcal{C}$, which is the ratio between the external electric field intensity to the internal electric field intensity. Note that $\mathcal{C}$ does not appear in the equations, but is needed for the boundary conditions for the 3D Laplace Eq. (11), $V_{\text{ex}}=\mathcal{C}V_{\text{in}}D/a$.

Here we could define the Reynolds number, which corresponds to the ratio of the inertial forces to the viscose forces; $\mathcal{R}=\rho a u_{\max}/\mu$, where $u_{\max}$ is the maximum velocity. By the dimensionless scaling applied in this paper, the Reynolds number is the same as the maximum nondimensional velocity magnitude.

Also, there is a difference in our nondimensional equations and those of other references on thin film electroconvection, which usually rescale time with the electric relaxation time. The reason this formulation is chosen is to obtain results which show explicitly that the dynamics becomes independent to conductivity in low Prandtl-like numbers. This point is explained in Sec. V.

IV. NUMERICAL SIMULATION

We constructed a time-stepping numerical simulation to solve the dimensionless governing equations. If the dynamics becomes steady in the iterative solution, the final steady answer to the equations is obtained. In specific cases with high forcing numbers, the iteration does not converge to a steady solution. This might be because of a real physical unsteady phenomenon (such as turbulent flows in high Reynolds numbers) or a numerical instability. In this paper, we focus on the cases in which a steady solution is found.

Our method for solving the hydrodynamics of this problem was based on a fully implicit scheme for the stream-function-vorticity formulation. We used a method similar to Ref. [40], which has solved the Navier-Stokes equations to solve the cavity flow problem and acceptable results were achieved. From the computational point of view, the hydrodynamics of this problem is similar to the cavity flow problem, in which

a closed loop advection is formed and numerical errors could be magnified when repeated in the loop. The elimination of pressure from the Navier-Stokes equations and decoupling of stream function and vorticity enables us to solve the set of equations for stream function and vorticity separately.

$$\frac{\partial \phi}{\partial t} = \frac{\partial^2 \phi}{\partial x^2} + \frac{\partial^2 \phi}{\partial y^2} + \omega, \tag{14}$$

$$\frac{\partial \omega}{\partial t} = \frac{\partial^2 \omega}{\partial x^2} + \frac{\partial^2 \omega}{\partial y^2} + \frac{\partial \phi}{\partial x}\frac{\partial \omega}{\partial y} - \frac{\partial \phi}{\partial y}\frac{\partial \omega}{\partial x} + \mathcal{F}\nabla \times (q\boldsymbol{E}). \tag{15}$$

Numerically, we calculate the time derivatives using explicit first-order approximation, and the other terms on the right-hand side are treated implicitly, with the derivatives centered in space and forward in time:

$$\frac{\partial c_{i,j}^n}{\partial t} = \frac{c_{i,j}^{n+1} - c_{i,j}^n}{\Delta t}, \tag{16}$$

$$\frac{\partial c_{i,j}^n}{\partial x} = \frac{c_{i+1,j}^{n+1} - c_{i-1,j}^{n+1}}{2\Delta x}, \tag{17}$$

$$\frac{\partial^2 c_{i,j}^n}{\partial x^2} = \frac{c_{i+1,j}^{n+1} - 2c_{i,j}^{n+1} + c_{i-1,j}^{n+1}}{\Delta x^2}. \tag{18}$$

Here the superscripts of n denote the time-step number, and i and j in the subscripts represent the position indices.

By applying this discretization, a system of L equations and L unknowns will be formed in each time step for each of the two hydrodynamic Eqs. (14) and (15). Here L is the number of grid points and the unknowns are the stream function and vorticity in the next time step, ϕ^{n+1} and ω^{n+1}, respectively. The equations are solved and the stream function and vorticity in the next time step are found. This implicit method is unconditionally stable, and provided that it leads to a steady solution, the solution is independent of the time step.

As mentioned, the body force that appears in the Navier-Stokes equation is resulted from the charge and electric field. For the electric calculation, we have the charge distribution in the present time step and should find the charge distribution in the next time step. The charge derivation is calculated according to Eq. (10). For this purpose, the relation between charge and potential on the film needs to be known, which is a consequence of Eq. (11); so if we have the charge distribution, it will be treated as a boundary condition for the 3D Laplace equation addressing the potential above the film, and by solving the equation, the potential will be found.

For this calculation, we made a 3D grid with the film positioned at the central part of its lower boundary. The geometry space has dimensions of $10 \times 10 \times 5$, as shown in Fig. 2. The two sides of this space along the y direction are assumed to be the capacitively coupled plates, and have the specific potentials $(\pm V_{\text{ex}}/2)$ as the boundary conditions. Also, the region that is supposed to be the conducting electrodes would have the specific voltage of $\pm V_{\text{in}}/2$ as boundary conditions. In each point on the liquid film that is a lower boundary of this 3D area, the boundary condition is a function of the charge density on the corresponding point. In this boundary condition, the gradient of electric potential is defined in Eq. (11). The rest of the boundaries are assumed

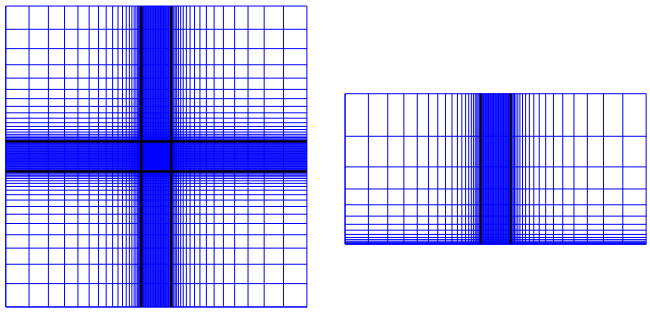

FIG. 2. (Color online) Top view (left) and side view (right) of the three-dimensional grid for calculation of the charge-potential relation. Dimensions of the box are $10 \times 10 \times 5$, the film being a 1×1 square at the bottom center of the box. The box has $83 \times 83 \times 43$ grid points, and the film is 43×43 points, uniform and square structured.

to have a normal potential gradient of zero. For each finite difference point in the computational space, there is one equation [Laplace Eq. (11)] and one unknown (3D potential in that point). For solving both the hydrodynamic and electric equations, we constructed the system of linear equations in the form of a sparse matrix and solved it using the built-in function *mldevide* in MATLAB, which solves the linear system using LU factorization with partial pivoting.

Since the Laplace equation is linear, we applied a superposition to simplify the calculation of the electric equations. So instead of solving the 3D Laplace equation in every iteration of the main solution, we first made a series of calculations with which the 4D matrix $\mathscr{A}$ was computed:

$$\psi_{i,j} = \sum_{k=1}^{M}\sum_{l=1}^{N} q_{i,j}\mathscr{A}_{i,j,k,l}. \tag{19}$$

The matrix $\mathscr{A}$ is then employed in the main solution, which demonstrates the charge-potential relation. So in each time step, having the charge distribution q^N, the potentials are calculated, and the charge distribution in the next time step is obtained by explicitly applying the advection term and the current divergence term:

$$q^{N+1} = q^N - (\boldsymbol{u}^N \cdot \nabla)q^N + \frac{1}{\mathcal{P}}\nabla^2\psi. \tag{20}$$

Therefore, the ultimate solution procedure is a repetition of time steps, in which the electrical equations are solved to find the charge and potential at the next time step, which will be used to compute the source term in the stream function vorticity formula. Next, the hydrodynamic equations are solved to find the stream function and vorticity in the next time step. The time-step sequences proceed until the solution converges to a steady state. The convergence criterion is based on defined residuals for stream function and charge. The residual for any quantity c at time step n is calculated as follows:

$$R_{\text{es}} = [\max(c^n - c^{n-1})/\max(c^n)]/\Delta t. \tag{21}$$

Here, "max" denotes the maximum value among all of the finite difference points. Convergence is assumed when both the residuals for charge and stream function are less than 10^{-4}. After convergence, the stream function is used to find velocity components for visualization and postprocessing.

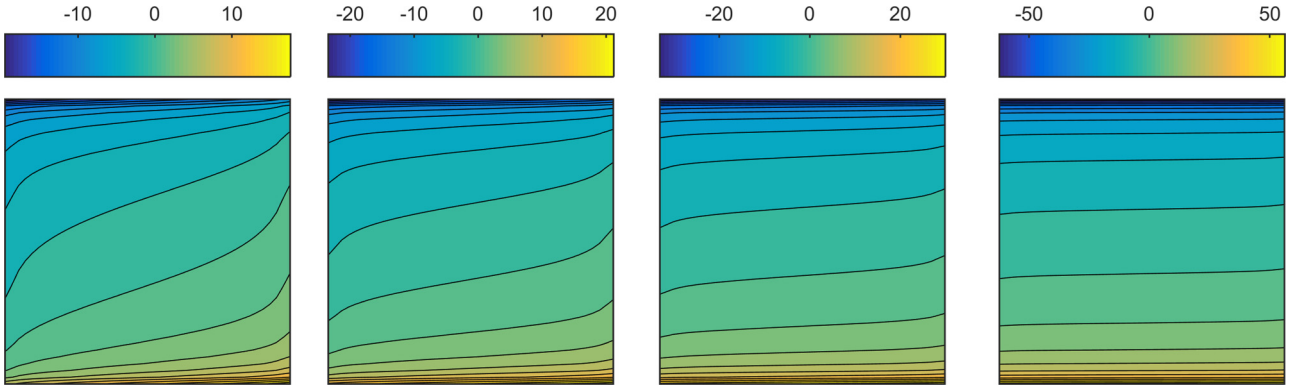

FIG. 3. (Color online) The base states: Contours of charge density for different field ratio numbers. Left to right: $\mathcal{C} = 2, 4, 10, 40$. The capacitively coupled plates are at the top (positive) and bottom (negative) sides of the film, and the conductive electrodes are at the right (positive) and left (negative) sides.

V. RESULTS AND DISCUSSION

The simulation was performed in different ranges of the dimensionless numbers and results are reported and discussed in this section. First the "Base state" for potential and charge distribution is discussed, then the low Prandtl-like number regime is explained, which is the case where the motion of the film does not change the charge distribution from its base state, and also the most common condition when experimenting with water-based solutions. Finally, the general case is discussed, in which the conductivity is not high enough to allow the consideration of a low Prandtl-like number regime. In this case the charge distribution is affected by the motion of the fluid, and all equations [Eqs. (8)–(11)] are involved in the final solution. The explanation in this order helps the understanding of the phenomenon step by step.

To be able to comprehend the conditions of the experiments, an estimation of the nondimensional numbers is made. The field ratio number $\mathcal{C}$ has usually been between 10 and 100. The force number $\mathcal{F}$ is usually between 10^2 and 10^6. The Prandtl-like number is a function of the material's conductivity. For water solutions, $\mathcal{P}$ was usually less than 10^{-7}.

A. Base state for potential and charge distribution

Assuming that there is no motion on the film or that the charge distribution on the film is not affected by the motion of the film, the nondimensional charge distribution and the potential on the entire film can be found only as a function of the field ratio $\mathcal{C}$. This is the case for the very small Prandtl-like numbers, as in Eq. (10) the advection term could be totally neglected. Understanding this charge distribution is an essential part of understanding the rotation mechanism.

Solving Eqs. (10) and (11) with the appropriate boundary conditions, the base state was calculated and is shown in Fig. 3.

B. Low Prandtl-like number regime

In the low $\mathcal{P}$ regime, the conductivity is so high that the charge distribution is not affected by the mechanical motion of the film. As explained before in Sec. II, in this case, changing the conductivity has no effect on the motion of the film. This is the usual case when experimenting with water-based solutions. The electrical charge distribution in this state is the same as the base state, which is only a function of the applied voltages, and is independent of the motion of the film and the Prandtl-like number (Fig. 3).

In this case, the motion is expected to be independent of the conductivity, as the electrical forces are caused by the charge distribution and the charge distribution would only be a function of the applied voltages and not the motion or the conductivity values. This assumption was verified by simulating the phenomenon in different $\mathcal{P}$ values. As explained in the next section, the differences between different results became negligible as the Prandtl-like number becomes less than 10^{-3}. Therefore, to simulate the low $\mathcal{P}$ condition, we eliminated the charge distribution calculation from each time step, and instead the steady charge distribution was calculated once at the beginning of the simulation.

To investigate the effect of the actuating forces on the motion, the dimensionless number $\mathcal{F}$ was varied, and the steady-state results were obtained. $\mathcal{F}$ is the ratio between the electrical forces to viscous forces. Low values for $\mathcal{F}$ indicate that the viscous forces are dominant. A series of simulation was performed with a constant field ratio $\mathcal{C}$ equal to 30. In this set, the force number $\mathcal{F}$ was varied in a range between 10^2 to 10^5. The dimensionless velocity magnitudes and vorticity increase as $\mathcal{F}$ increases, which is because the actuating forces inducing the motion increase. The relation between the maximum velocity and the force number obeys a quite linear trend in our simulation range, as illustrated in Fig. 6.

Several facts in the results agree with those of the experiments. The velocity profile is very similar to the experimental results, with velocity being zero at the edges and the center, and the maximum velocity encounters somewhere in the midway. Figure 4 shows a typical velocity vector field for our results, which is in agreement with those of the experiments [29].

As the results indicate, in the low Prandtl-like number regime the maximum velocity of the motion is directly proportional to the force number. It is also observed that as the force number increases, the streamlines of the motion tend to become circular as shown in Fig. 5. This is a result of domination of the advection term in the Navier-Stokes equations to the diffusion terms, which means that inertial

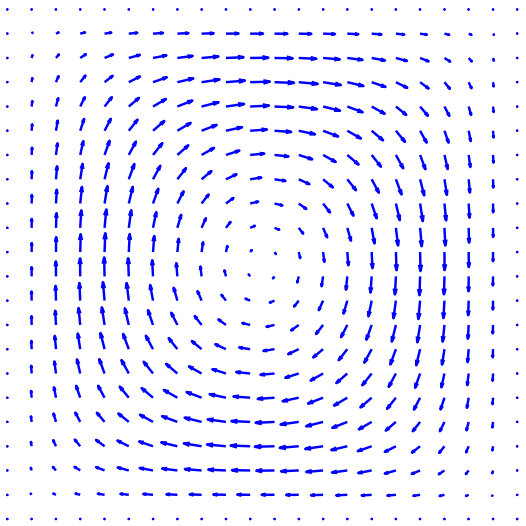

FIG. 4. (Color online) Typical form for a velocity vector field. $\mathcal{F} = 100$, $\mathcal{C} = 30$, and $\mathcal{P} = 10^{-8}$.

forces dominate viscous forces. In other words, in small force numbers, the velocity in a specific point is proportional to the electric force at the same point. As the force number increases, the Reynolds number also increases, therefore the fluid tends to maintain its velocity due to inertia, leading to a circular motion. Also, in higher Reynolds numbers, the behavior of the flow might become unsteady.

We also changed the field ratio $\mathcal{C}$ to observe its effect in the low Prandtl-like number regime. As explained in the previous subsection, in high-field ratio numbers $\mathcal{C}$, where the E_{ex} is much higher than the internal field, the charge distribution is a function of y; positive charges will be accumulated near the negative plate and vice versa. As the field ratio decreases, the charge distribution approaches to the corners, positive charges approaching to the positive electrodes, and vice versa. Figure 3 shows the base states of charge for different field ratios.

We simulated the low Prandtl-like number regime for $\mathcal{F} = 50$, and different field ratios from 1 to 50. We observed that changing $\mathcal{C}$ caused no noticeable change in the motion of the film; i.e., changing the internal and external voltages does not change the motion of the film provided that their product remains the same. This fact could be interpreted as follows: The body force inducing motion (vector field of $\boldsymbol{f}$) is a product of the electric field ($\boldsymbol{E}$) and the charge on the film (q). The electric field is directly proportional to the electrode voltages (V_{in}), and the capacitively coupled plates cannot cause an electric field inside the film. The charges are induced both by the electrodes and the capacitively coupled plates, and due to linearity of electric equations, can be assumed to be a sum of two charge distributions caused by the electrodes (q_{in}) and capacitively coupled plates (q_{ex}):

$$\boldsymbol{f} = \boldsymbol{E}(q_{\text{in}} + q_{\text{ex}}). \tag{22}$$

Now both $\boldsymbol{E}$ and q_{in} are symmetrical about the x-z plane, therefore their product cannot cause a nonsymmetrical rotation around the z axis. So it is the term $\boldsymbol{E} \cdot q_{\text{ex}}$ that should lead to rotation. $\boldsymbol{E}$ is linearly proportional to the conducting electrodes voltage and q_{ex} is linearly proportional to the external voltage. This could show why when the field ratio changes but the product of the voltages remain constant, the motion does not show a significant change in the low Prandtl-like number regime. Note that this conclusion is not valid for high Prandtl-like numbers, since both the voltages and charges would be affected by the motion of the film.

C. General case

So far we assumed that the charge distribution is the same as the base state, however, in fluids with conductivities much less than water, this assumption cannot be true. This is the case where the Prandtl-like number is very high, and the effect of fluid motion on charge distribution can no longer be neglected. We call this state the general case.

In the general case, the Prandtl-like number cannot be assumed to be very small, and thus the fluid motion affects the charge and potential distribution. It is the advection term in Eq. (10) $[(\boldsymbol{u} \cdot \nabla)\boldsymbol{q}]$ that causes the charge distribution to vary from its base state by the fluid motion. The greater the Prandtl-like number, the more the charge distribution is affected by the motion. At first, this effect changes the charge density distribution and the electric field intensity and direction, which usually reduces the effecting forces on the

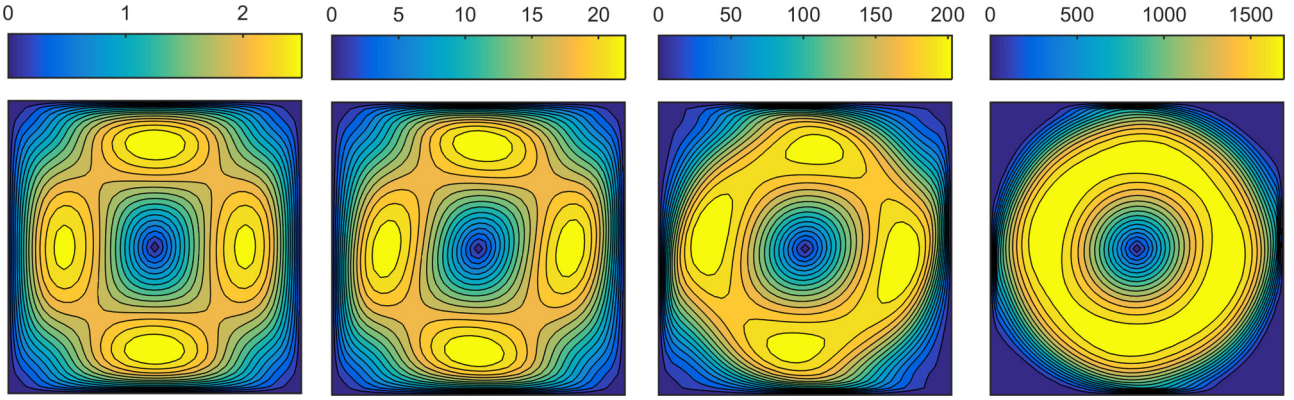

FIG. 5. (Color online) Contours of velocity magnitude for different force numbers $\mathcal{F}$. From left to right: $\mathcal{F} = 10^2, 10^3, 10^4$, and 10^5. $\mathcal{C} = 30$ and $\mathcal{P} = 10^{-8}$. Note that as the force number increases, the flow becomes advection dominated; therefore, inertial forces dominate leading to smooth circular flows.

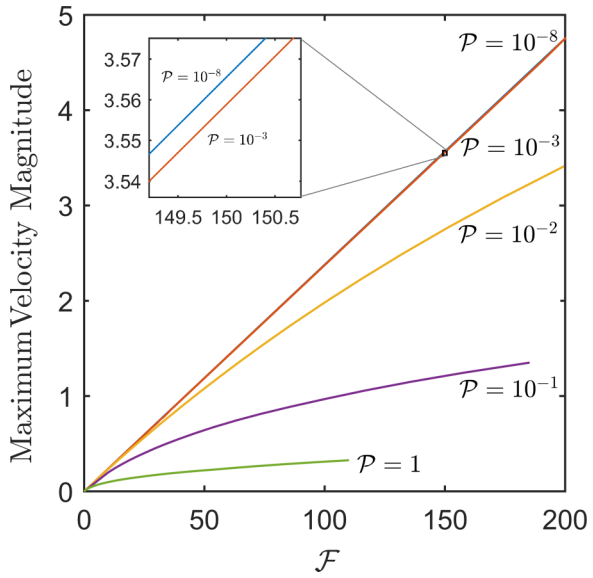

FIG. 6. (Color online) The relation between the maximum velocity and the force number $\mathcal{F}$ for different Prandtl-like numbers and $\mathcal{C} = 30$. In the low Prandtl-like number regime, the relation is linear and the result is independent of the Prandtl-like number. However, in high Prandtl-like numbers, the relation becomes nonlinear as the force number increases.

fluid, and slows the rotation as shown in Figs. 6 and 7. In small force numbers, the velocities are small, and thus the change of charge distribution becomes negligible. However, in large force numbers, the effect becomes significant. This leads to the nonlinear effect that is seen in the diagram.

As well as reducing the maximum velocity, the effect also changes the profile of the motion as shown in Fig. 8. The simulation results for different values of the nondimensional parameters are shown in Fig. 9. When the charges are dragged with the moving fluid, they tend to move back to their stable position. At the steady state, the deformation of the charge distribution leads to a rotation resisting effect, i.e., the motion of fluid near the sides displaces the charges, and a charge

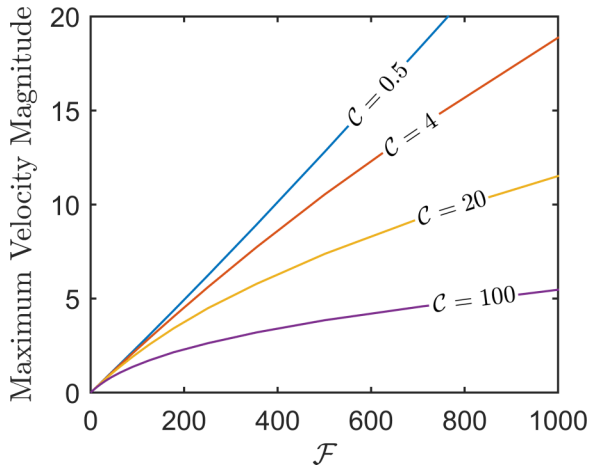

FIG. 7. (Color online) The relation between the maximum velocity and the force number $\mathcal{F}$ for different field ratios $\mathcal{C}$ and $\mathcal{P} = 10^{-2}$.

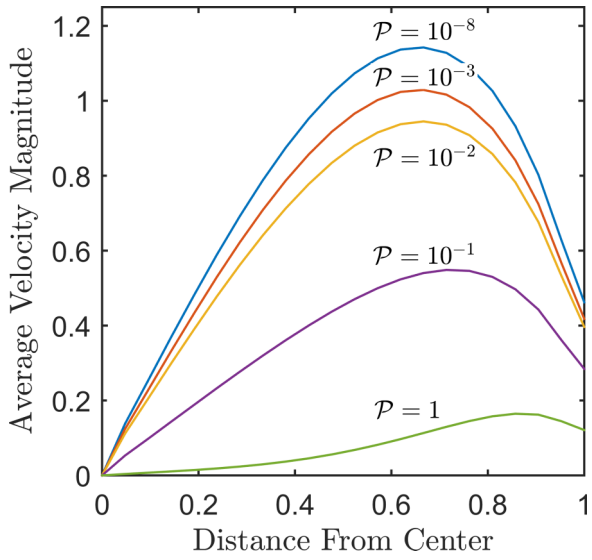

FIG. 8. (Color online) The velocity profile for $\mathcal{F} = 50$ and $\mathcal{C} = 30$. It is shown that increasing the Prandtl-like number tends to stop the motion from the center, leading to motion near the edges only.

motion at an inner layer exerts an opposite force, canceling the inner motion. As the Prandtl-like number increases, the effect cancels the motion at the center. As a result, in high Prandtl-like numbers and high enough force numbers, the motion velocity will be maximized somewhere near the edges of the film, and the center becomes stationary as shown in Fig. 8. Figure 7 shows the variation of velocity magnitude with the field ratio number $\mathcal{C}$. Increasing the field ratio number $\mathcal{C}$ increases the amount of charge density and increases the effect of charge distribution variation on motion. Also, when the force number $\mathcal{F}$ increases, since the velocity magnitude increases, again the deformation of charge distribution will be more significant, and the velocity incrementation will be different than the low Prandtl-like number regime.

This effect has already been observed clearly in experiments [29], that for poor conductive liquids (high $\mathcal{P}$), like 1-Bromo-3-fluorobenzene, and high enough field ratios, the maximum velocity regime approaches the sides of the film, and our results provide a theoretical explanation of this effect.

VI. CONCLUSION

We have derived the governing equations of the dynamics for the liquid film motor by following the well-known calculations on thin film electroconvection and electrohydrodynamics. A three-dimensional computer model is constructed, and simulation results illustrate the rotation mechanism of the liquid film motor. Free electrical charges are accumulated on the free surfaces of the film, both by the charge-conducting electrodes and the capacitively coupled plates. The internal electric field exerts a certain force to the charged film. The three-dimensional calculation is vital in the explanation of the accumulated charges.

Several experimental results are explained by this theory and simulation, a number of which have been explained for the first time. These results include the form of motion, including the no-slip boundary condition, the independency of motion

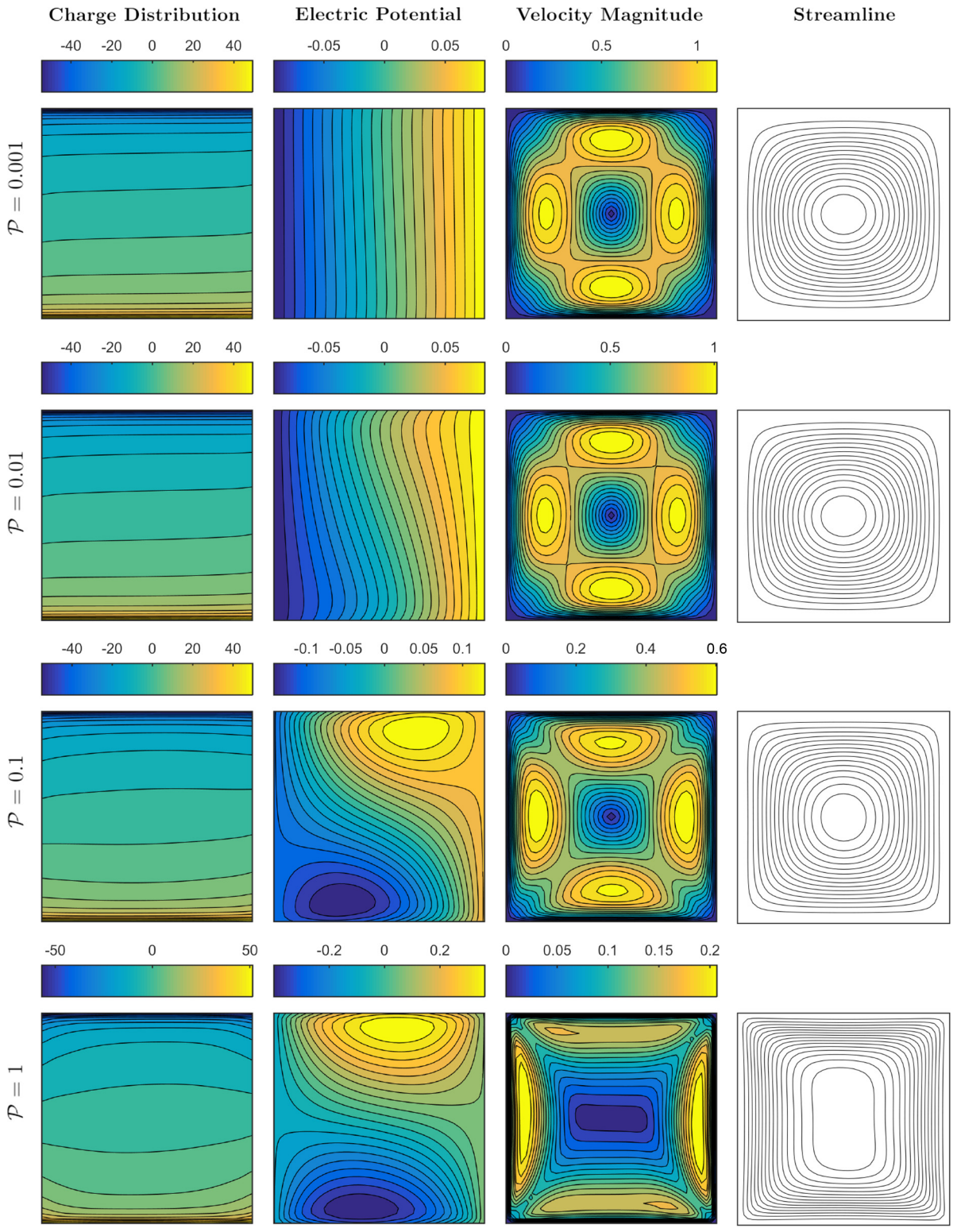

FIG. 9. (Color online) Effect of Prandtl-like number on the liquid film motor. Left to right: Contours of charge density, contours of electric potential, contours of velocity magnitudes, and streamlines. Top to bottom: $\mathcal{P} = 10^{-3}$, 10^{-2}, 10^{-1}, and 1. $\mathcal{C} = 30$ and $\mathcal{F} = 30$. As the Prandtl-like number increases, the charge distribution becomes more and more affected by the fluid motion. Therefore, potentials change from the base state, and so does the surface forces exerted to the fluid. The tendency of the fluid to become stationary at the center is a result of this complicated behavior.

to conductivity for conductive liquids like water (i.e., the low Prandtl-like regime), and the tendency of the fluid to move near the sides only for weakly conductive liquids.

Our theory relies on previously well-known principles, as in the electroconvection, and is consistent with other related phenomena, such as the liquid film electric generator.

ACKNOWLEDGMENTS

The authors thank Prof. S. W. Morris for his help on the idea and discussions about the theory and Prof. M. M. Namin for the help on the numerical methods and schemes. Also contributions of Prof. M. R. Ejtehadi, Dr. R. Shirsavar, and S. Amiri are acknowledged. This work was supported by Sharif Applied Physics Research Center.

[1] J. Plateau, *Statique Expérimentale et Théorique des Liquides Soumis aux Seules Forces Moléculaires*, Vol. 2 (Gauthier-Villars, Paris, 1873).
[2] J. W. Gibbs, *The Collected Works of J. Willard Gibbs*, Vol. 1 (Yale University Press, New Haven, CT, 1948).
[3] K. J. Mysels, *Soap Films: Studies of Their Thinning and a Bibliography* (Pergamon Press, Oxford, UK, 1959).
[4] C. Isenberg, *The Science of Soap Films and Soap Bubbles* (Courier Dover Publications, London, 1978).
[5] A. I. Rusanov and V. V. Krotov, Progr. Surface Membrane Sci. **13**, 415 (1979).
[6] G. Debrégeas, P. Martin, and F. Brochard-Wyart, Phys. Rev. Lett. **75**, 3886 (1995).
[7] J. Zhang, X. Wu, and N. Rashidnia, Phys. Fluids **18**, 085110 (2006).
[8] J. M. Chomaz and B. Cathalau, Phys. Rev. A **41**, 2243 (1990).
[9] J. Zhang, S. Childress, A. Libchaber, and M. Shelley, Nature **408**, 835 (2000).
[10] M. Gharib and P. Derango, Physica D: Nonlin. Phenom. **37**, 406 (1989).
[11] G. Boffetta and R. E. Ecke, Annu. Rev. Fluid Mech. **44**, 427 (2012).
[12] A. A. Sonin, *The Surface Physics of Liquid Crystals* (Taylor & Francis, London, 1995).
[13] J. C. Tarczon and K. Miyano, Phys. Rev. Lett. **46**, 119 (1981).
[14] C. Rosenblatt and N. M. Amer, Appl. Phys. Lett. **36**, 432 (2008).
[15] S. Faetti, L. Fronzoni, and P. Rolla, Le J. Physique Colloq. **40**, C3 (1979).
[16] S. Faetti, L. Fronzoni, and P. A. Rolla, J. Chem. Phys. **79**, 5054 (1983).
[17] S. Morris, Liquid Crystals Today **2**, 4 (1992).
[18] H. Pleiner, R. Stannarius, and W. Zimmermann, in *Evolution of Spontaneous Structures in Dissipative Continuous Systems* (Springer, Berlin, 1998), pp. 295–334.
[19] P. Tsai, Z. A. Daya, and S. W. Morris, Phys. Rev. E **72**, 046311 (2005).
[20] V. B. Deyirmenjian, Z. A. Daya, and S. W. Morris, Phys. Rev. E **72**, 036211 (2005).
[21] Z. A. Daya, V. B. Deyirmenjian, and S. W. Morris, Phys. Rev. E **64**, 036212 (2001).
[22] P. Tsai, Z. A. Daya, V. B. Deyirmenjian, and S. W. Morris, Phys. Rev. E **76**, 026305 (2007).
[23] P. Tsai, Z. A. Daya, and S. W. Morris, Phys. Rev. Lett. **92**, 084503 (2004).
[24] S. Ried, H. Pleiner, W. Zimmermann, and H. R. Brand, Phys. Rev. E **53**, 6101 (1996).
[25] V. B. Deyirmenjian, Z. A. Daya, and S. W. Morris, Phys. Rev. E **56**, 1706 (1997).
[26] Z. A. Daya, S. W. Morris, and J. R. de Bruyn, Phys. Rev. E **55**, 2682 (1997).
[27] C. Langer and R. Stannarius, Phys. Rev. E **58**, 650 (1998).
[28] A. Amjadi, R. Shirsavar, N. H. Radja, and M. Ejtehadi, Microfluid. Nanofluid. **6**, 711 (2009).
[29] R. Shirsavar, A. Amjadi, A. Tonddast-Navaei, and M. Ejtehadi, Exp. Fluids **50**, 419 (2011).
[30] R. Shirsavar, A. Amjadi, M. Ejtehadi, M. Mozaffari, and M. Feiz, Microfluid. Nanofluid. **13**, 83 (2012).
[31] A. Amjadi, M. S. Feiz, and R. M. Namin, Microfluidics and Nanofluidics **18**, 141 (2015).
[32] J. Melcher and G. Taylor, Annu. Rev. Fluid Mech. **1**, 111 (1969).
[33] E. V. Shiryaeva, V. A. Vladimirov, and M. Y. Zhukov, Phys. Rev. E **80**, 041603 (2009).
[34] I. Rubinstein and B. Zaltzman, Phys. Rev. E **62**, 2238 (2000).
[35] B. Zaltzman and I. Rubinstein, J. Fluid Mech. **579**, 173 (2007).
[36] Z.-Q. Liu, Y.-J. Li, G.-C. Zhang, and S.-R. Jiang, Phys. Rev. E **83**, 026303 (2011).
[37] Z.-Q. Liu, G.-C. Zhang, Y.-J. Li, and S.-R. Jiang, Phys. Rev. E **85**, 036314 (2012).
[38] Z. A. Daya, V. B. Deyirmenjian, and S. W. Morris, Phys. Fluids **11**, 3613 (1999).
[39] T. Saghaei, A.-R. Moradi, R. Shirsavar, and M. Habibi, Appl. Phys. Lett. **106**, 053506 (2015).
[40] E. Erturk, T. C. Corke, and C. Gökçöl, Int. J. Numer. Methods Fluids **48**, 747 (2005).